A novel carboxylesterase 2-targeted fluorescent probe with cholic acid as a recognition group for early diagnosis of drug- and environment-related liver diseases

Jingkang Li [a], Mo Ma [a,b], Zhimin Zhang [a], Lanlan Xu [a], Bin Yang [a], Quanping Diao [c], Pinyi Ma [a,*], Daqian Song [a,c,**]

[a] *College of Chemistry, Jilin Province Research Center for Engineering and Technology of Spectral Analytical Instruments, Jilin University, Qianjin Street 2699, Changchun 130012, China*
[b] *School of Pharmacy, Jilin University, Qianjin Street 2699, Changchun 130012, China*
[c] *Liaoning Key Laboratory of Development and Utilization for Natural Products Active Molecules, School of Chemistry and Life Science, Anshan Normal University, Anshan, China*

HIGHLIGHTS

- Probe LAN-CA selected cholic acid as a novel recognition group for CES2.
- Cholic acid is not only a recognition group, but also has a good hepatoenteric targeting ability.
- Probe LAN-CA effectively imaged hyperlipidemic cells and monitored their recovery process.
- LAN-CA was successfully used for diagnosing hepatoenteric diseases and monitoring NAFLD drug therapy.

GRAPHICAL ABSTRACT
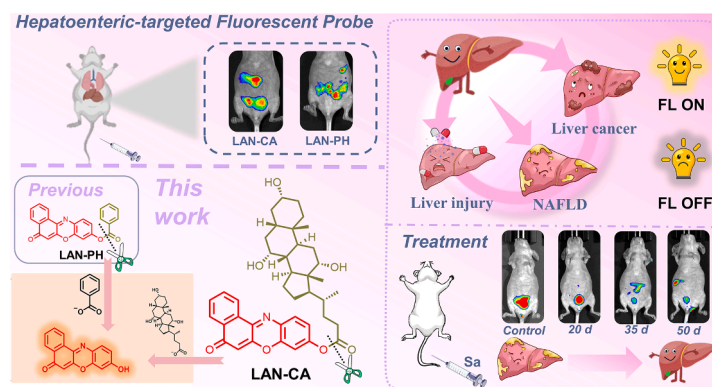
ARTICLE INFO

ABSTRACT

Due to the detrimental effects of various harmful substances—such as carcinogens, drug toxicity, and environmental pollutants—on the liver, which can trigger or exacerbate conditions like hepatocellular carcinoma (HCC), drug-induced liver injury (DILI), and non-alcoholic fatty liver disease (NAFLD), accurate detection and monitoring of these diseases are crucial for effective treatment. Carboxylesterase 2 (CES2) is primarily found in the liver and, as a potential biomarker, its accurate detection can enhance the early diagnosis and treatment efficacy of liver diseases. Traditional fluorescence probes for CES2 detection suffer from non-specific recognition groups, leading to poor targeting specificity. To address this limitation, we propose a novel CES2-responsive fluorescent

---

probe utilizing cholic acid (CA) as a recognition group. The probe, LAN-CA, was synthesized by esterifying CA with a near-infrared fluorophore, LAN-OH. This novel fluorescent probe leverages the unique affinity of CA for hepatocytes, ensuring that LAN-CA remains and accumulates specifically within the hepatoenteric circulation. *In vitro* experiments showed that the probe exhibits superior optical performance compared to traditional benzoate-based probe (LAN-PH), with a detection limit of 0.015 μg/mL. Examination of 56 common biological interferents demonstrated that using CA as a recognition group offers high selectivity. Cell experiments confirmed that LAN-CA is an effective tool for monitoring endogenous CES2 in live cells. Comprehensive evaluations of fluorescence imaging in various mouse models of liver diseases, such as HCC, DILI, and NAFLD, demonstrated that LAN-CA provides exceptional imaging accuracy and therapeutic monitoring capabilities. In conclusion, this probe not only can be a promising tool for accurate liver disease diagnosis, but also can provide valuable insights into treatment efficacy.

1. Introduction

The harmful effects of various toxic substances, such as carcinogens, drug toxicity, and environmental pollutants, can trigger or exacerbate liver diseases, including hepatocellular carcinoma (HCC), drug-induced liver injury (DILI), and non-alcoholic fatty liver disease (NAFLD) [1,2]. Therefore, accurate detection and monitoring of these conditions are crucial for effective treatment. Carboxylesterase 2 (CES2) is a key enzyme predominantly found in the liver, playing essential roles in drug metabolism, detoxification processes, and the hydrolysis of various endogenous and exogenous substrates [3–5]. Due to its substantial presence in hepatic tissues, CES2 has emerged as a promising biomarker for evaluating liver function and diagnosing liver-related diseases [6]. Traditional methods for detecting CES2 include a range of biochemical assays and imaging techniques that leverage the enzyme's ability to cleave ester bonds [7–9]. These methods often utilize benzoate ester-based probes, which react with CES2 to produce a detectable signal [10,11]. Among these techniques, fluorescence imaging stands out due to its real-time imaging capability, high sensitivity, and cost-effectiveness, making it the preferred method for CES2 detection in biological contexts [12–15]. However, these probes exhibit several limitations, particularly regarding their specificity for hepatic tissues.

One of the primary challenges with existing CES2 detection methods is their lack of targeting specificity [16]. The widespread presence of ester bonds in various tissues and organs can lead to off-target effects, reducing the precision of liver imaging [17]. This lack of specificity compromises the accuracy of liver disease diagnostics, as signals may originate from non-hepatic tissues, leading to false positives or misleading results. Consequently, there is a pressing need for the development of liver-specific enzyme-responsive fluorescence probes to enhance the precision and accuracy of liver disease diagnostics.

To address these limitations, this study introduces cholic acid (CA) as a novel recognition group for CES2. CA serves as a critical signaling molecule in various liver-associated pathways and possesses a unique affinity for hepatocytes, facilitating targeted delivery to these cells [18, 19]. Su et al. developed the hCy-CA-LAP probe responsive to leucine aminopeptidase (LAP), significantly enhancing the hepatocyte-targeting ability of the probe through the addition of CA moieties [20]. Extending from this approach, they utilized CA for precise in-situ imaging of acute inflammatory liver injury (AILI) and autoimmune hepatitis (AIH) in vivo, underscoring the efficacy of incorporating CA structures into probes for targeted liver diagnostics [21]. These studies underscore the efficacy of incorporating CA structures into probes for targeted liver diagnostics. However, the intricate synthesis steps and structural complexity that are required for probe construction pose certain challenges to the synthesis and practical application of the probes.

Given that CES2 can selectively cleave sterically hindered polar ester bonds, traditional probes based on benzoate esters fall short in targeting the liver. In this study, we used CA to develop a novel fluorescent probe for targeting CES2. We synthesized LAN-CA, a probe with specificity for CES2, by forming an ester bond between the carboxyl group of CA and a near-infrared fluorophore (LAN-OH) previously designed by our group.
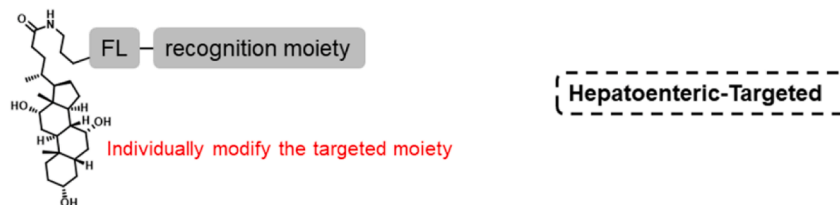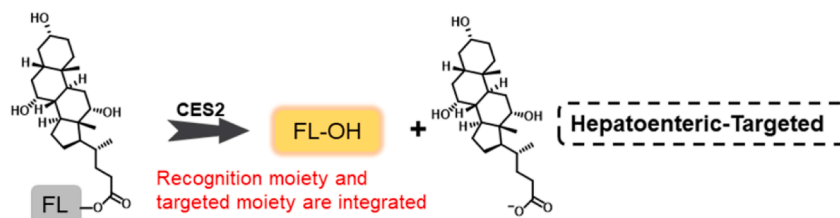

Scheme 1. Mechanism of enzyme digestion response.

The structural framework and application of this probe are illustrated in Scheme 1. Compared to conventional CES2 fluorescent probes using benzoate esters as recognition units, LAN-CA incorporates CA, which structurally resembles triterpene-like acids known to inhibit CES2, thereby significantly boosting the probe's selectivity for CES2 [22]. This design strategy simplifies the probe's architecture and intrinsically embeds it with liver-targeting capabilities.

To evaluate the effectiveness of the probe in CES2 detection and its liver-targeting capabilities, we selected liver disease models related to the intake of harmful substances, including HCC, DILI, and NAFLD, and employed LAN-CA for in situ liver imaging to further elucidate the relationship between liver diseases and CES2. Furthermore, to demonstrate its broad application, LAN-CA was employed to monitor the treatment process of NAFLD with specific medications.

2. Experimental methods

2.1. Materials and equipment

Detailed information on reagents and instruments is provided in the Supplementary Material. The synthesis route is depicted in Fig. 1. Comprehensive synthesis procedures for Compound 1, LAN-OH and LAN-PH are also available in the Supplementary Material.

Synthesis of LAN-OH. Compound 1 was synthesized according to the literature [23]. Compound 1 (304 mg, 2.2 mmol) and 1-naphthol (288 mg, 2 mmol) were dissolved in 10 mL CH_2Cl_2 and stirred evenly. Next 5 mL hydrochloric acid was added into the flask and stirred at room temperature overnight. The mixture was purified by silica gel chromatography (petroleum ether: ethyl acetate = 5:1). The compound LAN-OH was gained as dark red solid, 55 % yield. MS (LC-ESI-MS, m/z) for $C_{16}H_{10}NO_3^+$ [M+H]$^+$: calculated, 264.0655; found, 264.0650 (Fig. S1).

Synthesis of LAN-CA. Cholic acid (204 mg, 0.5 mmol) was dissolved in 15 mL of anhydrous DMF and while stirring, triethylamine (100 μL, 0.7 mmol) was added. After HBTU (266 mg, 0.7 mmol) was gradually added, the mixture was stirred for 1 h. Subsequently, LAN-OH (39 mg, 0.15 mmol) was introduced, the mixture was stirred at room temperature overnight. Upon completion of the reaction, the mixture was diluted with saturated NaCl solution and then extracted with ethyl acetate. The organic layer was separated, dried over anhydrous sodium sulfate, and concentrated under reduced pressure. Purification was carried out by silica gel column chromatography using dichloromethane:methanol (25:1) as an eluent, which yielded LAN-CA as a yellow solid with 21 % yield. ^{1}H NMR (600 MHz, DMSO-d_6) δ 8.65 (d, J
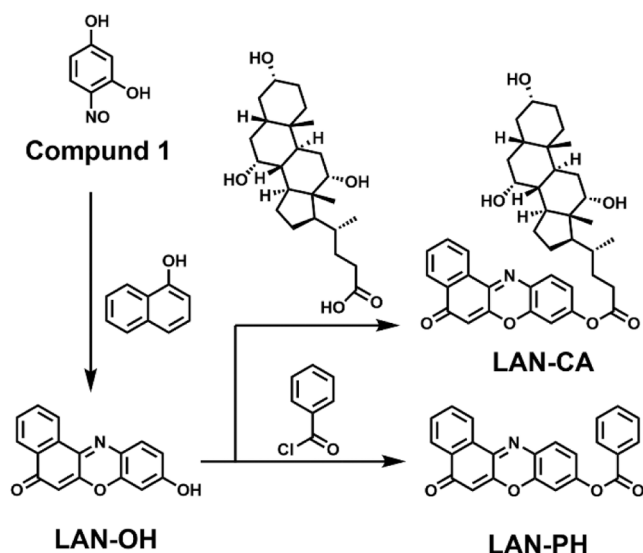
= 7.6 Hz, 1 H), 8.16 (d, J = 7.6 Hz, 1 H), 7.92 (t, J = 7.7 Hz, 2 H), 7.88 (s, 1 H), 7.38 (d, J = 2.4 Hz, 1 H), 7.23 (dd, J = 8.6, 2.4 Hz, 1 H), 6.45 (s, 1 H), 4.32 (s, 1 H), 4.17 – 4.00 (m, 4 H), 3.88 – 3.75 (m, 1 H), 3.18 (s, 1 H), 2.24 – 2.14 (m, 3 H), 2.04 – 1.98 (m, 2 H), 1.87 – 1.78 (m, 6 H), 1.66 (dd, 5 H), 1.55 – 1.18 (m, 6 H), 0.95 – 0.73 (m, 5 H), 0.61 (d, 5 H). ^{13}C NMR (DEPTQ) (151 MHz, DMSO-d_6) δ 183.24, 172.34, 152.90, 151.57, 147.02, 144.62, 132.88, 132.54, 132.04, 131.41, 130.74, 130.66, 125.74, 124.85, 119.81, 110.24, 107.04, 71.46, 70.90, 66.71, 51.64, 46.49, 46.29, 41.99, 41.88, 35.78, 35.50, 35.35, 34.87, 31.16, 30.90, 29.48, 29.02, 27.79, 26.70, 23.28, 23.10, 17.48, 12.82. MS (LC-ESI-MS, m/z) for $C_{40}H_{47}NO_7^+$ [M+H]$^+$: calculated, 654.3353; found: 654.3349 (Fig. S2, Fig. S3 and Fig. S4).

2.2. Detection of CES2 in solution

A 1 mM LAN-CA stock solution was prepared by solubilizing LAN-CA in DMSO. To determine the optimal test conditions, enzymatic reaction parameters were optimized.

Reaction time optimization. In the determination of optimal reaction time, the reaction mixture consisting of 0.2 μg/mL CES2 and 10 μM LAN-CA in phosphate-buffered saline (PBS) (10 mM, pH 7.4) was incubated at 37 °C for various durations (2, 8, 15, 25, 35, 45, 65, 90, 110, and 130 min).

pH optimization. The pH was optimized using reaction mixtures containing 0.2 μg/mL CES2 and 10 μM LAN-CA in PBS buffer at varying pH values (pH 4, 5, 6, 7, 7.4, 8, 9, and 10). Each mixture was incubated at 37 °C for 40 min

Temperature optimization. To determine the optimal reaction temperature, the reaction mixture consisting of 0.2 μg/mL CES2 and 10 μM LAN-CA in phosphate-buffered saline (PBS) (10 mM, pH 7.4) was incubated at various temperatures (25 °C, 30 °C, 37 °C and 40 °C) for 40 min

Probe selectivity. Under the optimal conditions, the selectivity of the probe was assessed. The reaction mixture containing 10 μM LAN-CA in PBS (10 mM, pH 7.4) was incubated at 37 °C for 40 min

Analytical methods. The prepared mixtures were analyzed using fluorescence spectrometry and UV-Visible spectrophotometry. Fluorescence measurements were conducted at an excitation wavelength of 575 nm to ensure the optimal detection sensitivity.

2.3. Establishment of cell model

To explore CES2 behavior in a high-fat context, HepG2 cells (human liver cancer cells) were employed. The cells were cultured on glass-bottom dishes for 24 h to allow for real-time imaging of CES2 activity. HepG2 cells were used in all experiments unless otherwise stated Cell imaging experiments were conducted on a Nikon AX laser scanning confocal microscope at an excitation wavelength of 580 nm. Additional methodological details are provided in the Supplementary Material [24–26].

CES2 dynamics in HepG2 cells. Initial experiments involved time-lapse imaging of HepG2 cells treated with 10 μM LAN-CA, and the CES2 dynamics over various time points were monitored.

Cellular endogenous CES2 imaging [7]. HepG2 cells were divided into four groups. Cells in the first group were incubated with 10 μM LAN-CA for 20 min before imaging control group. Cells in the second and third group were first pre-treated with 1 mM 5-FU/LPA, washed three times with PBS (10 mM, pH 7.4), and then incubated with 10 μM LAN-CA before imaging. To demonstrate that the subsequent use of liver therapeutics has no effect on the endogenous CES2 activity in normal HepG2 cells, we added the fourth group. Cells in the fourth group were first pre-treated with 50 μM saroglitazar, washed three times with PBS (10 mM, pH 7.4), and then incubated with 10 μM LAN-CA before imaging.

Imaging of CES2 in high-fat cells. The experimental setup comprised three distinct groups. The first group involved HepG2 cells being

Fig. 1. Synthetic route of LAN-CA and LAN-PH probes.

exposed for 48 h to a high-fat environment, consisting of 240 μM sodium oleate and 120 μM sodium palmitate [27]. Subsequently, the cells were washed thrice with PBS (10 mM, pH 7.4) and then incubated with 10 μM LAN-CA before imaging. This group aimed to evaluate the probe's performance in a lipid-rich context. In the second group, high-fat cells were treated with 50 μM therapeutic drugs (saroglitazar, Glu, GSH and NAC) for 16 h and then incubated with 10 μM LAN-CA before imaging. This group aimed to evaluate the efficacy of drug in the treatment of liver fat accumulation. The third group (control group) involved the treatment of HepG2 cells with 10 μM LAN-CA for 20 min prior to imaging to assess the probe's cellular uptake and localization under normal conditions.

2.4. Establishment of mouse model

All animal experiments were conducted in accordance with the ethical guidelines established by the Institutional Animal Care and Use Committee (IACUC) of Jilin University. The animal experimental ethical inspection permit number is SY202306031. A series of disease models were established based on mice (BALB/c-nu mice). The specific details are as follows:

Orthotopic liver cancer mouse model. A total of 1×10^7 HepG2 cells were suspended in 300 μL of PBS (10 mM, pH 7.4), and the suspension of HepG2 cells was then implanted into the liver of a mouse [28]. Orthotopic liver cancer mouse model was obtained on 15 days.

APAP-induced liver injury mouse model. N-acetyl-p-aminophenol (APAP) was dissolved in normal saline to a final concentration of 15 mg/mL. The mouse fasted overnight was intraperitoneally injected with 300 mg/kg of APAP solution [29]. The APAP-induced liver injury mouse model was obtained after 10 h.

NAFLD mouse model. A mouse model of NAFLD was developed following the methodologies reported in the literature [30]. The induction involved a two-week regimen of a methionine and choline-deficient diet to simulate high-fat dietary conditions.

Histological analyses, including Hematoxylin and Eosin (H&E) and Oil Red O staining, were employed to confirm the NAFLD phenotype, which includes hepatocyte swelling and disrupted hepatic architecture.

Treatment of mouse model. NAFLD mouse model was established according to the method described above [31]. The NAFLD mouse model was subjected to subsequent interventions, which involved the administration of saroglitazar (100 μL, 3 mg/kg) for 50 days. In a strategic temporal sequence, the mice received intravenous injections of LAN-CA on the 20th, 35th, and 50th days. A control group, which was given a standard diet and was untreated, was used as a benchmark for the therapeutic effects of the treatments.

3. Results and discussion

3.1. Spectral properties and reaction mechanism

The spectral properties of the probe LAN-CA were examined. As shown in the Fig. S5, it can be seen that the UV-Vis and fluorescence spectra of LAN-OH and LAN-CA are significantly different. As shown in Fig. 2 A, the addition of CES2 triggered a significant change in the solution color and a gradual increase in the fluorescence intensity. This observation could be ascribed to the CES2-catalyzed hydrolysis of LAN-CA, which causes the release of the hydroxyl group from the D-π-A structure, a robust electron donor. This reaction enhances the internal charge transfer (ICT) effect, thereby causing a substantial increase in the fluorescence intensity. Overall, the CES2 hydrolysis reaction facilitates the release of the phenolic hydroxyl group from LAN-OH, intensifying the ICT effect and markedly elevating the fluorescence intensity of the emission peak (λ_{emmax}) at 636 nm. To further validate the efficacy of LAN-CA, it was compared with LAN-PH, a traditional probe utilizing benzoate esters as a recognition moiety. At the same excitation wavelengths, despite the lower background fluorescence of LAN-PH before the addition of CES2, the fluorescence enhancement of LAN-CA after
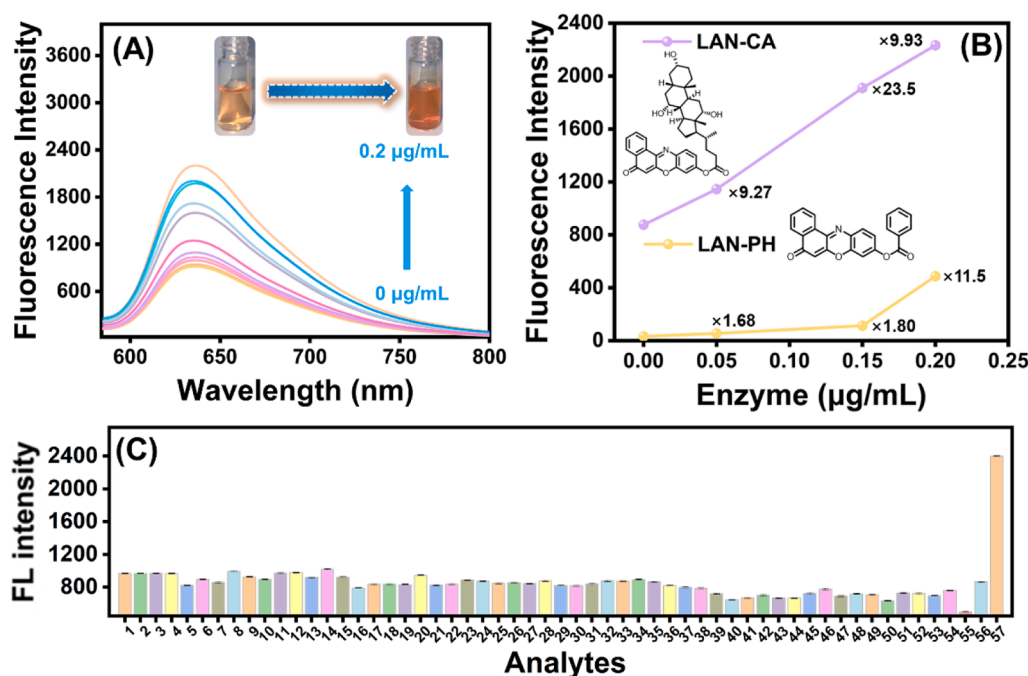

Fig. 2. (A) Fluorescence spectra (λ_{emmax} = 636 nm) of reaction solution (10 μM LAN-CA and 0 - 0.2 μg/mL CES2). (B) Comparison of fluorescence spectra (λ_{emmax} = 636 nm) of the two probes. (C) Fluorescence intensity of 10 μM LAN-CA in the presence of various analytes (1 mM, unless otherwise stated). 1–8: γ-glutamyl-transferase (GGT, 20 U/L), CES1 (0.5 μg/mL), glucose oxidase (20 U/mL), dipeptidyl peptidase IV (DPP-IV, 50 μg/mL), acetylcholinesterase (AChE,12 U/mL), butyrylcholinesterase (BChE, 12 U/mL), aminopeptidase N (APN, 25 U/mL), leucine arylamidase (LAP, 25 U/mL); 9–20: different anions (Br⁻, ONOO⁻, Cl⁻, ClO₄⁻, CN⁻, F⁻, H₂PO₄⁻, HPO₄²⁻, HSO₄⁻, I⁻, SCN⁻, SO₃²⁻); 21–38: cations (Ag⁺, Al³⁺, Ba²⁺, Ca²⁺, Cd²⁺, Co²⁺, Cu²⁺, Fe²⁺, Fe³⁺, Hg²⁺, K⁺, Li⁺, Mg²⁺, Mn²⁺, Na⁺, Ni²⁺, Pb²⁺, Zn²⁺); 39–54: amino acids and proteins (Asp, Cys, GSH, Hcy, His, Ser, Tyr, Val, Phe, Ala, Met, Gly, Glu, Arg, Lys, Leu); 55:H⁺ (1 mM); 56: OH⁻ (1 mM) were added to the solution as a disturbance group.

CES2 addition was more pronounced, the indication of its enhanced response sensitivity (Fig. 2B). Additionally, we assessed the selectivity of LAN-CA towards CES2. The results, as presented in Fig. 2 C, the other 54 bioactive substances, as well as acidic and alkaline environments, had no significant effect on LAN-CA, underscored the remarkable CES2 specificity of the probe when cholic acid was employed as the recognition moiety. These results confirm the suitability of cholic acid as CES2-specific recognition group, exhibiting that it has reaction capabilities comparable to those of traditional recognition groups.

The sensing mechanism of LAN-CA for CES2 was investigated using a multifaceted approach, including HPLC-MS analysis, theoretical calculations, and molecular docking simulations. The findings, as illustrated in Fig. S6, revealed a notable decrease in the intensity of the mass peak of LAN-CA (m/z 654.3352) upon the introduction of CES2, and this was accompanied by the emergence of the mass peak of LAN-OH (m/z 264.0593). Further HPLC analysis, as detailed in Fig. S7, identified the characteristic peaks of the reaction system at 1.28 min and 3.44 min, which align with the peaks of LAN-CA and LAN-OH, respectively. These observations corroborate the sensing mechanism depicted in Fig. 3 A, confirming that LAN-CA was hydrolyzed to LAN-OH through CES2-mediated hydrolysis.

The luminescence mechanism was elucidated through theoretical calculations. As demonstrated in Fig. 3B, the electrostatic potential results indicated that LAN-OH had a more pronounced charge transfer capability compared to LAN-CA. This suggests that the hydrolysis of LAN-CA by CES2 enhances the ICT effect, leading to a significant increase in the fluorescence signal. Finally, the molecular docking experiments provided additional information, confirming that the probe can efficiently target the CES2 recognition site. As depicted in Fig. 3 C, the molecular docking simulation revealed that LAN-CA forms three hydrogen bonds with CES2, which specifically involves three amino acids: ARG208, GLN212, and MET244. These interactions have a low binding energy of −12.4 kcal/mol, an indication of a strong binding affinity of LAN-CA towards CES2. The data highlight the probe's ability to effectively bind to its target enzyme.

3.2. Analytical performance of LAN-CA

To evaluate the analytical performance of LAN-CA, various test conditions including reaction time, pH, and temperature, were meticulously optimized. The detailed discussions are available in the SI. The optimal conditions were as follows: reaction time, 40 min; pH, 7.4; and temperature, 37 °C. Under these optimal conditions, the relationship between the fluorescence intensity of LAN-CA solution (λ_{emmax} = 636 nm) and CES2 concentration was investigated. As illustrated in Fig. S8, the fluorescence intensity gradually increased in response to the increase in CES2 concentration. Notably, a robust linear correlation (R^2 = 0.996) was observed at the CES2 concentration ranging from 0.025 to 0.2 ng/mL. This shows that the probe is highly sensitive to CES2 at this concentration range. The detection limit of LAN-CA was further assessed and compared with that of other probes reported in the literature (Table S1) [4,5,32–34]. The assessment showed that LAN-CA had an exceptionally low detection limit (LOD = 0.015 µg/mL). The determination of LOD is detailed in the SI. These results underscore the high sensitivity of LAN-CA and its potential in applications aiming at CES2 detection.

3.3. Imaging of LAN-CA in cells

The cytotoxicity of LAN-CA was assessed using a CCK-8 assay. The assessment revealed that the cell survival rate exceeded 90 % (Fig. S9), which is indicative of minimal cytotoxicity of LAN-CA. Hemolysis tests further confirmed that LAN-CA had high biocompatibility, as evidenced by its low hemolysis rate (Fig. S10).

The dynamics of LAN-CA within HepG2 cells were scrutinized, from which we observed rapid cellular penetration and a gradual increase in fluorescence intensity that became stabilized at 20 min (Fig. S11). This suggests that LAN-CA possesses a swift response time for intracellular imaging. The specificity of the fluorescence signal to endogenous CES2 was confirmed through experiments involving inhibitors and activators. In control experiments, HepG2 cells were incubated with LAN-CA pre-treated with LPA (a CES2-specific inhibitor), and a marked reduction in fluorescence intensity was observed. Conversely, cells pre-treated with the activator 5-FU exhibited the enhancement of fluorescence signals (Fig. S12). These findings corroborate that the enhancement of fluorescence of LAN-CA is caused by endogenous CES2. This establishes LAN-CA as a potent tool for monitoring CES2 activity in live cells. In addition, APAP-induced liver injury and high-fat cell models were established, as shown in Fig. S13. The fluorescence intensity was significantly reduced, demonstrating down-regulation of CES2 expression in both disease species in the cell model.

The ability of LAN-CA to monitor CES2 fluctuations in a high-fat cell model was evaluated. Fluorescence intensity of high-fat cells was notably lower compared to that of normal cells. This suggests that
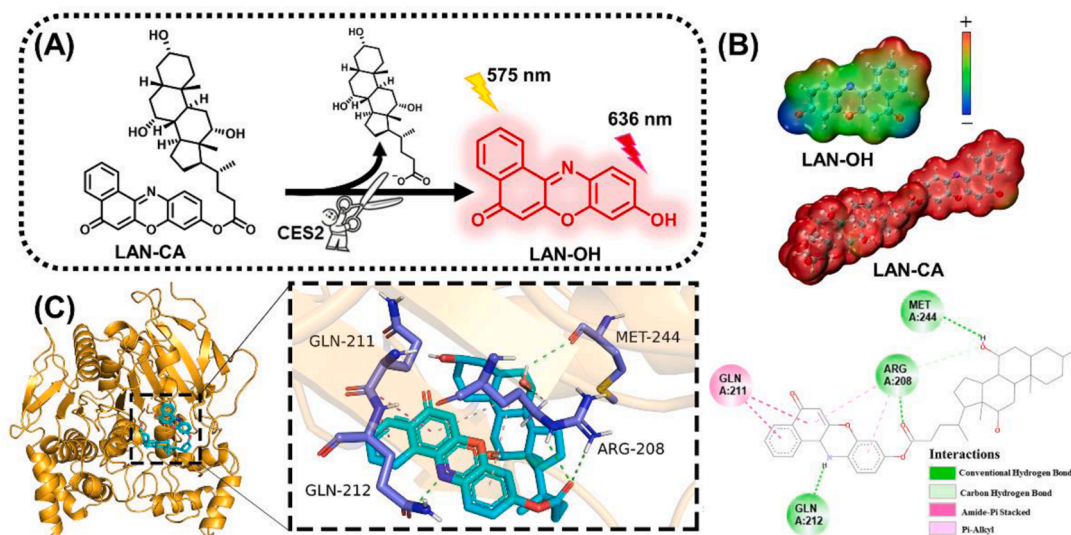

Fig. 3. (A) Schematic diagram of enzyme digestion reaction. (B) Electrostatic potential distribution of LAN-OH and LAN-CA. (C) Molecular docking simulation for the binding between LAN-CA and CES2.

excessive intracellular lipids can suppress CES2 expression, which aligns with the findings reported in the literature [35]. The therapeutic potential of saroglitazar, Glu, GSH, and NAC in a high-fat environment was explored, with a particular focus on the efficacy of saroglitazar in treating NAFLD. The cytotoxicity of saroglitazar was assessed using a CCK-8 assay. The assessment revealed that the cell survival rate exceeded 90 % (Fig. S14), which is indicative of minimal cytotoxicity of saroglitazar. In the post-treatment of hyperlipidemic cells with these drugs, a restoration of red fluorescence was observed (Fig. 4), which highlights the therapeutic impact. Specifically, as indicated by the fluorescence intensity ratio, the effectiveness of saroglitazar was superior to that of other drugs, underscoring its prominence as a treatment for high-fat conditions. Overall, these results underscore the high of sensitivity of LAN-CA to CES2 activity in hepatocytes, rendering it a valuable tool for evaluating the drug efficacy in treating liver diseases.

3.4. Imaging of mice with hepatic disease

Building on the encouraging outcomes of cellular experiments, we extended the application of LAN-CA to in vivo biological imaging. Prior research has illustrated the pathway in which cholic acids are actively secreted by liver cells through the intestine, demonstrating their involvement in the digestive system [36]. Subsequently, these acids are reabsorbed at the ileum, either through active or passive mechanisms, and then transported back to the liver via the portal vein. In the liver, they are processed and undergo transformation before being re-secreted into the small intestine along with newly synthesized cholic acids to facilitate the enterohepatic circulation [37]. Given this context, the LAN-CA compound, which has a cholic acid-like structure, possesses the ability to not only specifically recognize CES2, but also target the liver and intestine.

To demonstrate its hepatic and intestinal targeting capability in vivo, LAN-CA was compared with a traditional probe containing benzoate residues as the CES2 recognition moiety. As illustrated in Fig. 5 A, the fluorescence signal at the liver site of mice injected with LAN-CA gradually intensified over time. At 40 min post-injection, the fluorescence signal was prominently distributed in both the liver and intestine. In contrast, mice injected with LAN-PH exhibited a more dispersed fluorescence signal across the abdominal region without the evidence of targeting. For more accurate verification, anatomic imaging was performed on mice. As can be seen in Fig. S15, it is obvious that the fluorescence imaging of LAN-CA is obviously enriched in the liver and intestine, relatively speaking, the fluorescence signal distribution of LAN-PH is relatively scattered, and the fluorescence signal can not be ignored in other organs. The dynamic process caused by LAN-CA indicates that upon intravenous injection, the probe initially recognizes CES2 in the intestine. Over time, the enterohepatic circulation facilitates the movement of the cholic acid-like probe towards the liver. As a result, targeted imaging of both regions was achieved. These experimental

outcomes confirm the effective targeting capabilities of LAN-CA, suggesting its potential in the more precise detection and diagnosis of hepatic and intestinal diseases.

In addition, to investigate the metabolism of the probe in mice, we monitored the fluorescence signal for 24 h post-injection. As shown in Fig. S16, a strong fluorescence signal was detected within the first 4 h after injection. The signal then gradually weakened by the 8 h mark, and no obvious fluorescence signal was observed after 24 h. These results indicate that once the probe enters the hepatoenteric circulation, it is gradually metabolized, and the cleaved fluorophore is ultimately fully metabolized and excreted from the body within 24 h.

We established mouse models for DILI, HCC and NAFLD and used them in the investigation of the potential application of LAN-CA across different diseases [28–31].

Liver injury, often triggered by harmful substances such as drugs, environmental toxins, and pollutants, can result in significant hepatocyte damage. In the context of DILI, the hepatotoxic effects of certain medications can lead to liver damage and dysfunction, which directly impacts the liver's ability to synthesize and secrete enzymes like CES2 [38,39]. Our study utilized a DILI mouse model induced by APAP to explore the application of LAN-CA in detecting early liver damage. Compared to that of normal mice, the fluorescence intensity in the liver of mice with liver injury markedly decreased, indicating a reduction of CES2 due to hepatocyte damage (Fig. 5 C). This finding underscores LAN-CA's potential for early detection of liver injury related to drug toxicity.

HCC, a primary liver cancer, is another condition closely associated with exposure to carcinogenic substances such as aflatoxins and environmental pollutants. In contrast, the fluorescence signals at hepatic and intestinal sites of mice with liver cancer were significantly increased. This is likely attributed to the aberrant expression of CES2 in cancer cells [40]. The enhanced fluorescence signals in the liver and intestine of mice with liver cancer align with the findings reported in the literature [7]. The enhanced signals indicated an abnormal CES2 activity associated with liver cancer cells (Fig. 5D), highlighting LAN-CA's potential for detecting CES2 dysregulation in cancerous tissues.

NAFLD is a quintessential metabolic disorder that can disrupt the enterohepatic circulation system [41]. This condition is often exacerbated by exposure to environmental pollutants and other harmful substances, which contribute to lipid accumulation and liver inflammation.

We constructed a mouse model of NAFLD through high-fat diet induction. Post-intravenous injection of LAN-CA into mice, as depicted in Fig. 6 C, the liver region of the mice displayed negligible fluorescence signals, whereas the intestinal region exhibited strong fluorescence signals. This observation is likely caused by the hydrolysis of triglycerides in hepatocytes by CES2, leading to triglyceride depletion. In response to the progression of NAFLD, insulin sensitivity in the liver increases, and the intestine excessively secretes CES2 [35]. Consequently, the liver of NAFLD mouse cannot significantly consume the
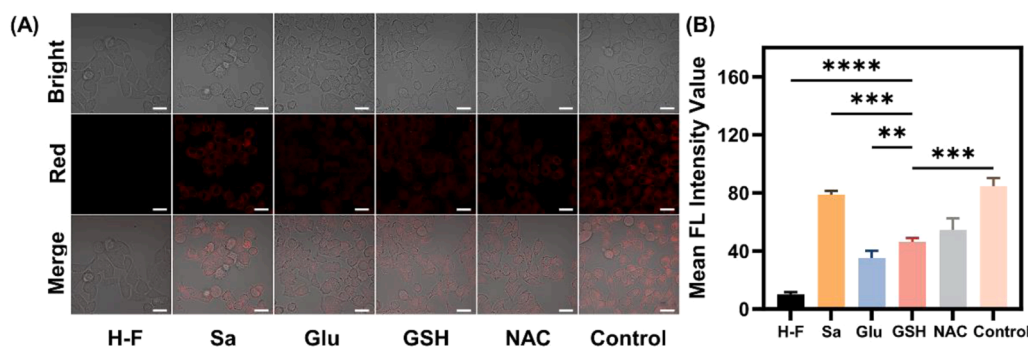

Fig. 4. (A) Fluorescence imaging of untreated high-fat cells (H-F) and high-fat cells treated with drugs (saroglitazar (Sa), Glu, GSH, and NAC). (B) Mean fluorescence intensity of cells in (A). Scale bar = 50 μm.
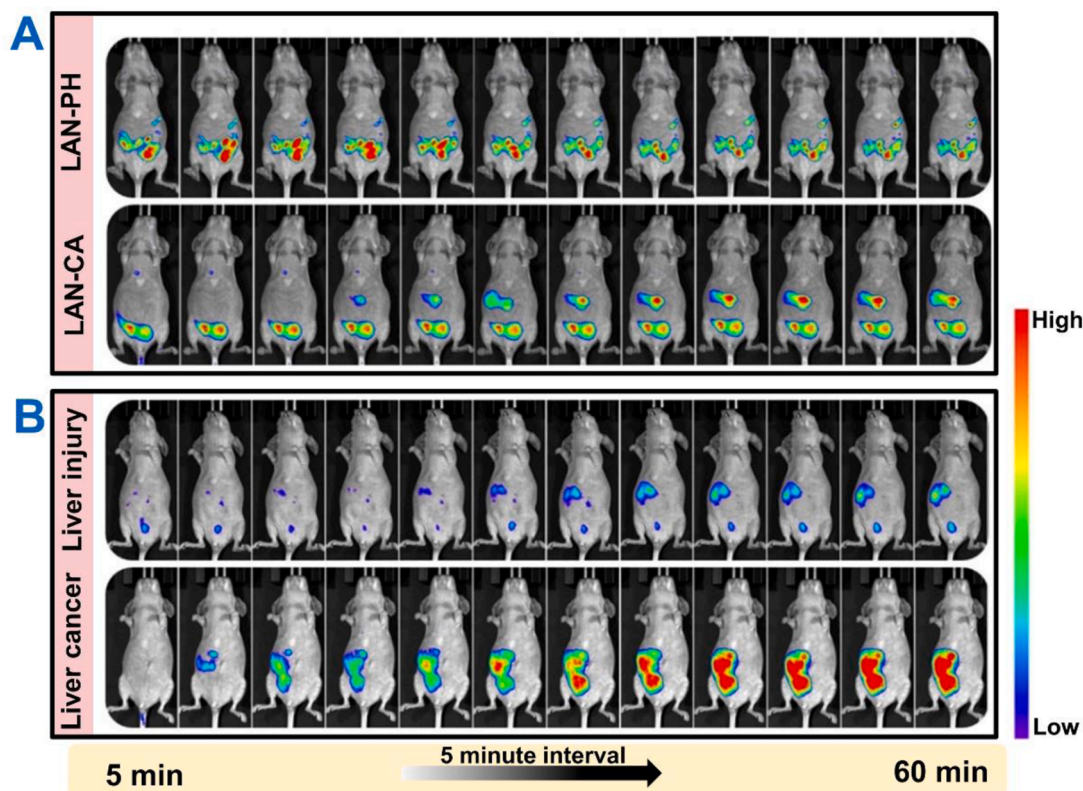
Fig. 5. (A) *In vivo* imaging of liver of normal mouse after intravenous (IV) injection with LAN-PH and LAN-CA (images were captured every 5 min for 60 min). (B) *In vivo* imaging of liver of mouse with liver injury(induced by APAP) and orthotopic liver cancer after IV injection with LAN-CA (in situ hepatoma model).

probe; instead, the probe is predominantly utilized in the intestine during the enterohepatic circulation process. As a result, the red fluorescence in the intestinal region was more pronounced. Dissection of the mice post-injection further confirmed the strong fluorescence in the intestinal area (Fig. 6 G), which aligns with the in vivo imaging results. These findings demonstrate LAN-CA's effectiveness in tracking disease progression and CES2 activity in the context of NAFLD, offering insights into how metabolic disorders affect liver and intestinal interactions.

To further assess the potential of LAN-CA in imaging diseases during treatment, we treated NAFLD mice with saroglitazar, a drug known for its efficacy in treating high-fat diet-induced conditions [31]. Preliminary cell experiments verified that saroglitazar neither significantly inhibited nor promoted CES2 activity; however, it could effectively restore high-fat-diet cells to their normal state. In this study, a NAFLD mouse model received saroglitazar injection (100 μL, 3 mg/kg). The treatment effects on the mouse were monitored over 20, 35, and 50 days, as illustrated in Fig. 6D-F. The observations revealed a continuous decrease in the brightness of intestinal fluorescence during the ongoing treatment, followed by a gradual recovery of the liver fluorescence. Dissecting the mice at 50 days post-treatment and after probe injection revealed the localization of fluorescence in the liver and intestinal regions (Fig. 6H), corroborating the success of in vivo imaging.

Subsequent dissection of the mice used in the disease and treatment studies was carried out. Compared to those of normal mice, the livers of NAFLD mice were visibly yellow and enlarged (Fig. 6I). Additionally, histological examinations using Hematoxylin and Eosin (H&E) staining and Oil Red O staining (Fig. 6B) revealed marked swelling, hepatic disarray, and lipid accumulation in the liver tissues of NAFLD mice. Moreover, the liver tissues of mice treated with saroglitazar were largely reverted to a state akin to that of healthy mice, which affirms the efficacy of saroglitazar in reversing fatty liver conditions (Fig. 6B). The outcomes indicated that the high-fat diet induction method was successfully employed to provoke substantial lipid accumulation in the

liver, thereby effectively establishing a NAFLD mouse model. After 50 days of treatment with saroglitazar, the liver returned to its normal state, as evidenced by the staining results. Compared with normal mice, as shown in Fig. S17, the recovery of liver fluorescence intensity was almost the same as that of normal mice. These findings are consistent with the monitoring results obtained using the LAN-CA probe, demonstrating that the probe not only can diagnose liver diseases such as NAFLD, but also can accurately monitor the severity of NAFLD. This alignment between histological analysis and probe-based imaging also underscores the potential of LAN-CA in both the diagnosis and precise monitoring of the progression of liver diseases.

This study confirms the hepatoenteric circulation of our probe and its ability to effectively detect changes in CES2 activity in the liver and intestine. Furthermore, it is the first study to demonstrate that CES2 activity in the liver and intestine is inversely correlated with non-alcoholic fatty liver disease, offering new insights into the pathophysiology of NAFLD and the potential therapeutic role of CES2 modulation.

This study confirms the hepatoenteric circulation of our probe and its ability to effectively detect changes in CES2 activity in the liver and intestine. Furthermore, it is the first study to demonstrate that CES2 activity in the liver and intestine is inversely correlated with NAFLD, particularly in the context of exposure to harmful substances. This finding offers new insights into the pathophysiology of NAFLD and highlights the potential therapeutic role of CES2 modulation in mitigating the effects of toxic environmental and dietary factors.

4. Conclusion

This study introduces a novel fluorescent probe, LAN-CA, designed with a specific recognition group for CES2. By incorporating CA as the CES2-targeting group, LAN-CA exhibits enhanced specificity for liver and intestinal enzymes. The molecular design leverages the unique affinity of CA for hepatocytes, allowing LAN-CA to specifically respond to
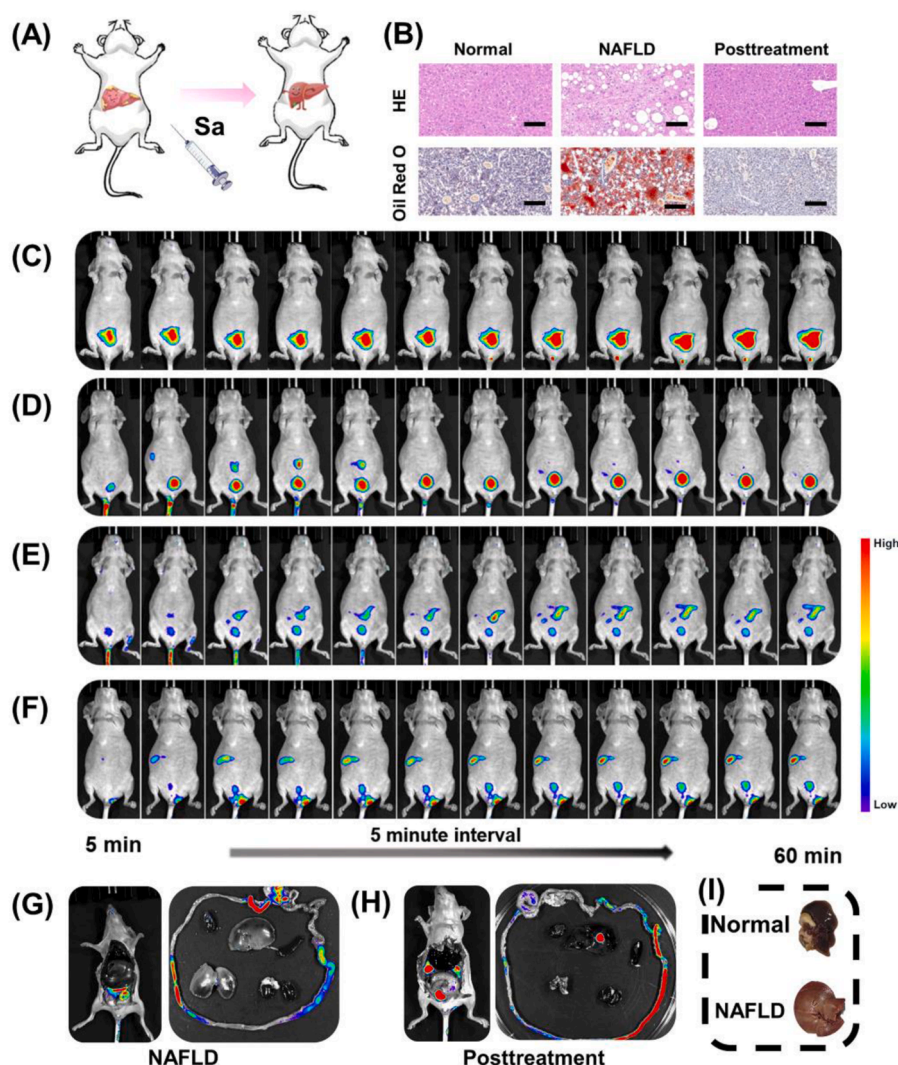
Fig. 6. (A) Diagrammatic illustration for the monitoring of treatment scheme of the NAFLD model. (B) H&E and Oil red O staining of liver tissues of normal mouse, NAFLD mouse and NAFLD mouse after treatment with saroglitazar for 50 days. Scale bar = 100 μm. (C) *In vivo* imaging of liver of NAFLD mice after intravenous (IV) injection with LAN-CA. (D), (E) and (F) *In vivo* imaging of liver of normal and NAFLD mice treated with saroglitazar for 20, 35 and 50 days after IV injection with LAN-CA. (G) and (H) Anatomic images of of untreated NAFLD mouse and NAFLD mouse treated with saroglitazar for 50 days after IV injection of LAN-CA. (I) Photographs of a healthy liver and an NAFLD liver.

CES2 activity by producing changes in the fluorescence signal. *In vivo* imaging results demonstrated that, following intravenous administration, LAN-CA specifically accumulated in the liver due to its targeted properties. This accumulation was confirmed using mouse models of various liver diseases. Particularly in models associated with harmful substances, such as DILI, HCC, NAFLD, LAN-CA effectively visualized changes in CES2 activity, providing critical insights into the impact of toxic environmental and dietary factors on liver function. Compared to traditional fluorescent probes, LAN-CA's organ-targeting capabilities provide not only accurate diagnostics for liver diseases but also a means to visualize treatment efficacy. The probe's ability to detect changes in fluorescence signals in the liver offers significant advantages for monitoring the progression and treatment of NAFLD. Overall, LAN-CA offers potential new approaches for diagnosing and monitoring liver diseases, particularly those influenced by harmful substances. Its targeting specificity and diagnostic accuracy suggest it could complement or replace traditional fluorescent probes, providing improved capabilities for assessing disease severity and monitoring therapy.

CRediT authorship contribution statement

Zhimin Zhang: Investigation, Data curation. **Mo Ma:** Investigation, Data curation. **Bin Yang:** Software, Formal analysis. **Lanlan Xu:** Investigation, Data curation. **Jingkang Li:** Writing – original draft, Validation, Investigation, Data curation, Conceptualization. **Pinyi Ma:** Writing – review & editing, Software, Project administration, Data curation. **Quanping Diao:** Software, Conceptualization. **Daqian Song:** Supervision, Resources, Project administration, Funding acquisition.

Declaration of Competing Interest

The authors declare that they have no known competing financial interests or personal relationships that could have appeared to influence the work reported in this paper.

Data availability

Data will be made available on request.

Acknowledgments

Appendix A. Supporting information

Supplementary data associated with this article can be found in the online version at doi:10.1016/j.jhazmat.2024.135966.

References

[1] Greenhill, C., 2018. New pathways in development of liver cancer. Nat Rev Gastro Hepat 15, 718-718.

[2] Ray, K., 2018. A complex interplay between inflammation and immunity in liver cancer. Nat Rev Gastro Hepat 15, 3.

[3] Feng, L., Liu, Z.M., Hou, J., Lv, X., Ning, J., Ge, G.B., et al., 2015. A highly selective fluorescent ESIPT probe for the detection of human carboxylesterase 2 and its biological applications. Biosens Bioelectron 65, 9–15.

[4] Feng, L., Liu, Z.M., Xu, L., Lv, X., Ning, J., Hou, J., et al., 2014. A highly selective long-wavelength fluorescent probe for the detection of human carboxylesterase 2 and its biomedical applications. Chem Commun 50, 14519–14522.

[5] Liu, Z.M., Feng, L., Hou, J., Lv, X., Ning, J., Ge, G.B., et al., 2014. A ratiometric fluorescent sensor for highly selective detection of human carboxylesterase 2 and its application in living cells. Sens Actuator B Chem 205, 151–157.

[6] Kisseleva, T., 2017. The origin of fibrogenic myofibroblasts in fibrotic liver. Hepatology 65, 1039–1043.

[7] Li, J.X., Cao, J.R., Wu, W., Xu, L.L., Zhang, S.Q., Ma, P.Y., et al., 2023. A molecular imaging tool for monitoring carboxylesterase 2 during early diagnosis of liver-related diseases. Sens Actuator B Chem 377, 133122.

[8] Yang, B., Ding, X.D., Zhang, Z.M., Li, J.K., Fan, S.Y., Lai, J.Y., et al., 2024. Visualization of production and remediation of acetaminophen-induced liver injury by a carboxylesterase-2 enzyme-activatable near-infrared fluorescent probe. Talanta 269, 125418.

[9] Wang, X.C., Gao, J., Fan, C.F., Gao, Y.K., Yang, X.T., Chen, L.X., 2024. New near-infrared fluorescence imaging platform with large stokes shift for carboxylesterase 2 detection in thyroid cancer and inflammatory diseases diagnosis. Anal Chem 96, 3772–3779.

[10] Wang, L.X., Wang, L.Y., Sun, X., Fu, L.L., Sun, M.Z., Wang, X.L., et al., 2024. Imaging of carboxylesterase 2 expression changes in colitis and colon cancer chemotherapy via a fluorescent probe. Sens Actuator B Chem 409, 135609.

[11] Yang, B., Ding, X.D., Li, J.K., Lai, J.Y., Zhang, Z.M., Xu, X.H., et al., 2023. Dihydroxanthene-derived fluorescent probe with near-infrared excitation and emission maxima for detecting human carboxylesterase-2 and bioimaging. Sens Actuator B Chem 395, 134503.

[12] Zeng, S., Wang, Y., Chen, C., Kim, H., Liu, X.S., Jiang, M.J., et al., 2024. An ER-targeted, viscosity-sensitive hemicyanine dye for the diagnosis of nonalcoholic fatty liver and photodynamic cancer therapy by activating pyroptosis pathway. Angew Chem Int Ed, e202316487.

[13] He, L., He, L.H., Xu, S., Ren, T.B., Zhang, X.X., Qin, Z.J., et al., 2022. Engineering of reversible NIR-II redox-responsive fluorescent probes for imaging of inflammation in vivo. Angew Chem Int Ed 61, e202211409.

[14] Li, H.D., Kim, D., Yao, Q.C., Ge, H.Y., Chung, J., Fan, J.L., et al., 2021. Activity-based NIR enzyme fluorescent probes for the diagnosis of tumors and image-guided surgery. Angew Chem Int Ed 60, 17268–17289.

[15] Wu, X.F., Wang, R., Kwon, N., Ma, H.M., Yoon, J., 2022. Activatable fluorescent probes for in situ imaging of enzymes. Chem Soc Rev 51, 450–463.

[16] Liu, S.Y., Zou, X.T., Guo, Y., Gao, X., 2022. A highly sensitive and selective enzyme activated fluorescent probe for in vivo profiling of carboxylesterase 2. Anal Chim Acta 1221, 340126.

[17] Tian, X.G., Yan, F., Zheng, J.Y., Cui, X.L., Feng, L., Li, S., et al., 2019. Endoplasmic reticulum targeting ratiometric fluorescent probe for carboxylesterase 2 detection in drug-induced acute liver injury. Anal Chem 91, 15840–15845.

[18] Zhou, X.M., Levin, E.J., Pan, Y.P., McCoy, J.G., Sharma, R., Kloss, B., et al., 2014. Structural basis of the alternating-access mechanism in a bile acid transporter. Nature 505, 569–573.

[19] Watanabe, M., Houten, S.M., Mataki, C., Christoffolete, M.A., Kim, B.W., Sato, H., et al., 2006. Bile acids induce energy expenditure by promoting intracellular thyroid hormone activation. Nature 439, 484–489.

[20] Zhang, Y., Chen, X.Q., Yuan, Q., Bian, Y.N., Li, M.R., Wang, Y.L., et al., 2021. Enzyme-activated near-infrared fluorogenic probe with high-efficiency intrahepatic targeting ability for visualization of drug-induced liver injury. Chem Sci 12, 14855–14862.

[21] Zhang, Y., Li, W., Chen, X.Q., Xiong, S.Q., Bian, Y.N., Yuan, L., et al., 2023. Liver-targeted near-infrared fluorescence/photoacoustic dual- modal probe for real-time imaging of in situ hepatic inflammation. Anal Chem 2579–2587.

[22] Wang, D.D., Zou, L.W., Jin, Q., Hou, J., Ge, G.B., Yang, L., 2018. Human carboxylesterases: a comprehensive review. Acta Pharm Sin B 8, 699–712.

[23] Xu, L.L., Chu, H.Y., Gao, D.J., Wu, Q., Sun, Y., Wang, Z.X., et al., 2023. Chemosensor with ultra-high fluorescence enhancement for assisting in diagnosis and resection of ovarian cancer. Anal Chem 95, 2949–2957.

[24] Ghanbari, M., Salavati-Niasari, M., Mohandes, F., 2021. Injectable hydrogels based on oxidized alginate-gelatin reinforced by carbon nitride quantum dots for tissue engineering. Int J Pharm 602, 120660.

[25] Ghanbari, M., Salavati-Niasari, M., Mohandes, F., Firouzi, Z., Mousavi, S.D., 2021. The impact of zirconium oxide nanoparticles content on alginate dialdehyde-gelatin scaffolds in cartilage tissue engineering. J Mol Liq 335, 116531.

[26] Ghanbari, M., Salavati-Niasari, M., Mohandes, F., 2021. Thermosensitive alginate-gelatin-nitrogen-doped carbon dots scaffolds as potential injectable hydrogels for cartilage tissue engineering applications. RSC Adv 11, 18423–18431.

[27] Tao, T., Zhang, Q., Liu, Z.B., Zhang, T., Wang, L.Y., Liu, J., et al., 2021. Polygonum cuspidatum extract exerts antihyperlipidemic effects by regulation of PI3K/AKT/FOXO3 signaling pathway. Oxid Med Cell Longev 2021, 3830671.

[28] Sun, T.T., Han, J.F., Liu, S., Wang, X., Wang, Z.Y., Xie, Z.G., 2019. Tailor-made semiconducting polymers for second near-infrared photothermal therapy of orthotopic liver cancer. ACS Nano 13, 7345–7354.

[29] Sun, M.D., Chen, P.Y., Xiao, K., Zhu, X., Zhao, Z.B., Guo, C.Y., et al., 2023. Circulating cell-free DNAs as a biomarker and therapeutic target for acetaminophen-induced liver injury. Adv Sci 10, e202206789.

[30] Radhakrishnan, S., Ke, J.Y., Pellizzon, M.A., 2020. Targeted nutrient modifications in purified diets differentially affect nonalcoholic fatty liver disease and metabolic disease development in rodent models. Curr Dev Nutr 4, nzaa078.

[31] Jain, M.R., Giri, S.R., Bhoi, B., Trivedi, C., Rath, A., Rathod, R., et al., 2018. Dual PPAR/agonist saroglitazar improves liver histopathology and biochemistry in experimental NASH models. Liver Int 38, 1084–1094.

[32] Liu, S.Y., Zou, X.T., Guo, Y., Gao, X., 2022. A highly sensitive and selective enzyme activated fluorescent probe for in vivo profiling of carboxylesterase 2. Anal Chim Acta 1221, 340126.

[33] Liu, X.Y., Li, X.Q., Dong, P., Wu, Z.M., Gao, J.W., Wang, Q.M., 2020. Near-infrared emission tracks inter-individual variability of carboxylesterase-2 via a novel molecular substrate. Microchim Acta 187, 313.

[34] Zhang, X.Y., Liu, T.T., Liang, J.H., Tian, X.G., Zhang, B.J., Huang, H.L., et al., 2021. A highly selective near infrared fluorescent probe for carboxylesterase 2 and its biological applications. J Mater Chem B 9, 2457–2461.

[35] Li, Y.Y., Zalzala, M., Jadhav, K., Xu, Y., Kasumov, T., Yin, L.Y., et al., 2016. Carboxylesterase 2 prevents liver steatosis by modulating lipolysis, endoplasmic reticulum stress, and lipogenesis and is regulated by hepatocyte nuclear factor 4 alpha in mice. Hepatology 63, 1860–1874.

[36] Ding, L., Yang, L., Wang, Z.T., Huang, W.D., 2015. Bile acid nuclear receptor FXR and digestive system diseases. Acta Pharm Sin B 5, 135–144.

[37] Trauner, M., Fuchs, C.D., Halilbasic, E., Paumgartner, G., 2017. New therapeutic concepts in bile acid transport and signaling for management of cholestasis. Hepatology 65, 1393–1404.

[38] Chalhoub, G., Kolleritsch, S., Maresch, L.K., Taschler, U., Pajed, L., Tilp, A., et al., 2021. Carboxylesterase 2 proteins are efficient diglyceride and monoglyceride lipases possibly implicated in metabolic disease. J Lipid Res 62, 100075.

[39] Zhang, C.L., Xu, Y.J., Gao, P., Lu, J.L., Li, X.P., Liu, D., 2015. Down-regulation of carboxylesterases 1 and 2 plays an important role in prodrug metabolism in immunological liver injury rats. Int Immunopharmacol 24, 153–158.

[40] Xu, G., Zhang, W., Ma, M.K., McLeod, H., 2001. Human carboxylesterase 2 is commonly expressed in tumor tissue and is correlated with activation of irinotecan. Clin Cancer Res 7, 3736S.

[41] Kanwal, F., Kramer, J.R., Mapakshi, S., Natarajan, Y., Chayanupatkul, M., Richardson, P.A., et al., 2018. Risk of hepatocellular cancer in patients with non-alcoholic fatty liver disease. Gastroenterology 155, 1828–1837.